Acta Biomaterialia 189 (2024) 286–297

Contents lists available at ScienceDirect

Acta Biomaterialia

journal homepage: www.elsevier.com/locate/actbio

Full length article

Elucidating the unexpected cell adhesive properties of agarose substrates. The effect of mechanics, fetal bovine serum and specific peptide sequences

Francesco Piazza[a], Beatrice Ravaglia[a], Andrea Caporale[b,c], Ana Svetić[d,e], Pietro Parisse[e,f], Fioretta Asaro[g], Gabriele Grassi[h], Luca Secco[a], Riccardo Sgarra[a], Eleonora Marsich[h], Ivan Donati[a], Pasquale Sacco[a,*]

[a] Department of Life Sciences, University of Trieste, Via Licio Giorgieri 5, I-34127 Trieste, Italy
[b] CNR, Institute of Crystallography, I-34149 Trieste, Italy
[c] CIRPeB, Research Centre on Bioactive Peptides "Carlo Pedone", University of Naples "Federico II", I-80134 Napoli, Italy
[d] Department of Physics, University of Trieste, Via Alfonso Valerio 2, I-34127 Trieste, Italy
[e] Elettra Sincrotrone Trieste S.C.p.A., s.s. 14km 1635 in Area Science Park, I-34149 Trieste, Italy
[f] Istituto Officina dei Materiali (CNR-IOM), Consiglio Nazionale delle Ricerche, s.s. 14km 1635 in Area Science Park, I-34149 Trieste, Italy
[g] Department of Chemical and Pharmaceutical Sciences, University of Trieste, Via Licio Giorgieri 1, I-34127 Trieste, Italy
[h] Department of Medical, Surgical and Health Science, University of Trieste, Strada di Fiume 447, I-34129 Trieste, Italy

ARTICLE INFO

Article history:
Received 21 May 2024
Revised 2 September 2024
Accepted 24 September 2024
Available online 30 September 2024

Keywords:
Agarose
Cell adhesion
Fetal bovine serum
RGD motif
Mechanobiology

ABSTRACT

2D agarose substrates have recently been surprisingly shown to be permissive for cell adhesion, depending on their mechanics and the use of the adhesive proteins of fetal bovine serum (FBS) in the cell culture medium. Here, we elucidate how the cells exhibit two anchoring mechanisms depending on the amount of FBS. Under low FBS conditions, the cells recognize the surface-coupled adhesive sequences of fibronectin via the binding of the heterodimer $\alpha_5\beta_1$ integrin. Functionality of the actomyosin axis and mechanoactivation of focal adhesion kinase (FAK) are essential for the stretching of the protein, thereby accessing the "synergy" PPSRN site and enhancing cell adhesion in combination with the downstream RGD motif. Under high FBS conditions, the specific peptide sequences are much less relevant as the adsorbed serum proteins conceal the coupled fibronectin and the cells recognize the adhesive protein vitronectin, which is constitutively present in FBS, via the binding of the heterodimer $\alpha_v\beta_3$ integrin. Similarly, the intracellular tension and FAK activity are decisive, which collectively indicate that the cells stretch the partially cryptic RGD site of vitronectin and thus make it more accessible for integrin binding. Both anchoring mechanisms only work properly if the agarose substrate is mechanically compliant in terms of linear stress-strain response, unraveling a critical balance between the mechanics of the agarose substrate and the presentation of the adhesive peptides.

Statement of significance

In the context of biomaterial design, agarose hydrogels are known to lack intrinsic cell-adhesive peptide motifs and are therefore commonly used for the development of non-permissive 2D substrates. However, we unexpectedly found that agarose hydrogels can become permissive substrates for cell adhesion, depending on a compliant mechanical response of the substrate and the use of fetal bovine serum (FBS) as protein reservoir in the cell culture medium. We describe here two anchoring mechanisms that cells harness to adhere to agarose substrates, depending on the amount of FBS. Our results will have a major impact on the field of mechanobiology and shed light on the central role of FBS as a natural source of adhesive proteins that could promote cell anchoring.

* Corresponding author.
E-mail address: psacco@units.it (P. Sacco).

https://doi.org/10.1016/j.actbio.2024.09.042

1. Introduction

Living tissues in the human body are physical microenvironments consisting of cells and the surrounding extracellular matrix (ECM). The interactions between cells and ECM play a pivotal role in embryonic development, differentiation, tissue remodeling and diseases such as fibrosis and cancer [1]. A well-accepted current concept is that of bidirectional relationship between cells and the ECM, *i.e.* mechanoreciprocity [2]. The cells transmit forces directly to the ECM via the "motor-clutch" actin-myosin-integrin axis or expanding their volume [3–6], and respond to physical inputs of the ECM such as stiffness, viscoelasticity and deformation, establishing a reciprocal feedback loop. ECM mimics in the form of hydrogels, which are mainly used in mechanobiology studies to recapitulate living microenvironments, often do not have intrinsic integrin binding sites, which hinders the interaction of cells and ECM and thus the transmission of cell forces. Therefore, chemical coupling of peptide sequences to these networks is a useful way to enable the adhesion of cells and control their fate decisions [7–12].

Among the polymers screened as ECM mimics, agarose is a polyagarobiose derived from marine red algae and consists of an alternation of d-galactose and 3,6-anhydro-l-galactose monomers linked by α-(1→3) and β-(1→4) glycosidic bonds [13]. Given the known gelling properties, non-toxicity and easily tunable mechanics of the resulting hydrogels depending on the molecular weight and chemical composition of the biopolymer, its concentration, the temperature quenching of the solutions and the thermal history of the hydrogels [14–20], agarose networks are currently used as a useful platform for tissue engineering and mechanobiology studies. In accordance with the above, agarose has no intrinsic cell-adhesive motifs and is therefore frequently used for the development of non-permissive 2D substrates for the generation of cell spheroids [21–23] or 3D networks for physical cell confinement studies [4]. Different chemical strategies have been devised over the years to couple or blend peptide sequences, especially the arginine-glycine-aspartic acid (RGD) motif, to agarose to improve cell adhesion [24–29].

Recently, we have shown that agarose hydrogels can become permissive 2D substrates for cell adhesion even without coupled RGD [16,18,30] and found that this is strictly dependent on two main features: a compliant mechanical response of the substrate and the use of fetal bovine serum (FBS) as a protein reservoir in the cell culture medium. In terms of mechanical properties, we have found that the methylation pattern and content of agarose and temperature quenching of its solutions after autoclaving sensitively alters the linear elasticity of the bulk network under oscillatory shear, which has been shown to be a key material trait for regulating cell adhesion [16,18]. As for the serum in the cell culture medium, we have shown that FBS is essential for triggering cell anchoring, and this occurs via the actin-myosin-integrin axis, which is supported by microtubule tension [30]. Taken together these findings, there is a synergistic interplay between substrate mechanics and the presence of serum proteins that promotes cell adhesion on compliant agarose substrates.

Considering that the FBS used in standard cell cultures (typically 10 % V/V) is rich in cell-adhesive proteins such as fibronectin and vitronectin [31,32] and more abundant non-adhesive proteins such as albumin (BSA) [33,34], the effect of these proteins in FBS *versus* the effect of specific peptide sequences coupled to hydrogel substrates in promoting cell adhesion cannot be neglected. This is particularly important considering that non-adhesive proteins such as BSA, cytochrome C or osteonectin have been shown to help expose in human fibronectin the hidden "synergy" integrin-binding site proline-histidine–serine-arginine-asparagine (PHSRN) [35] that enhances cell adhesion in combination with the RGD motif [36]. Nevertheless, the amount of FBS in cell culture media is of considerable biological relevance, as it plays a role in the physiology of mitochondria, for example [37]. The question now arises as to whether and how FBS in combination with specific adhesive sequences coupled to the surface of the agarose substrate and its mechanics jointly play a role in orchestrating cell adhesion. Here we report that FBS may or may not conceal specific peptide adhesive sequences coupled to the surface of agarose substrates, depending on its concentration. Therefore, cells respond to these specific sequences or adsorbed FBS, entailing different anchoring mechanisms. In both cases, the cells are able to firmly attach to the substrate and spread. However, this only applies if the agarose substrates are mechanically compliant in terms of linear stress-strain response of the bulk network.

2. Materials and methods

2.1. Agarose source

Agarose from *Gracilaria* was kindly provided by Java Biocolloid (Trieste, Italy). Agarose from *Gelidium* (Oxoid Agar Bacteriological) was purchased from Thermofisher Scientific. Agarose sample for electrophoresis (EP, code EMR920500) was purchased from Euroclone, Italy. The physical-chemical characteristics of the agaroses used in this study have been previously described [18] and reported in the Tables S1 and S2 in the Supplementary Material.

2.2. Preparation of agarose hydrogels

Agarose powder from EP, *Gracilaria* and *Gelidium* was added to PBS buffer (NaCl 8 g/L; KCl 0.2 g/L; Na_2HPO_4 • 2 H_2O 1.44 g/L; KH_2PO_4 0.24 g/L; pH 7.4) with vigorous stirring to achieve a final concentration of 0.9 % w/V for EP, 1 % w/V for *Gracilaria* and 1.2 % w/V for *Gelidium*. The preliminary results show that increasing the biopolymer concentration in both *Gracilaria* and *Gelidium* makes it possible to compensate for the higher sulfated agaropectin content (see Table S1), which is known to reduce the strength of the agarose hydrogel by affecting the assembly of helices [38]. This allows us to set the same elastic modulus ($G' \sim 6$ kPa) for the three hydrogel systems investigated under oscillatory shear. Agarose suspensions were autoclaved ($T = 121$ °C) and the resulting solutions were quenched at 85 °C for 10 min and then at 60 °C for 10 min before being poured into cylindrical supports [16]. The solutions were then allowed to gel at room temperature for 30 min and finally the hydrogels were incubated at 37 °C for 24 h under water-saturated conditions to equilibrate the system [14]. The final hydrogels exhibit very similar transparency, as determined by turbidity measurements (Fig. S3, Supplementary Material).

2.3. Rheological characterization

Rheological characterization of the hydrogel disks (20 mm in diameter and 2–2.5 mm thick) was performed by means of an HAAKE MARS III rheometer (ThermoScientific) operating at $T = 37$ °C with cross-hatched parallel plate configuration. During the measurements, a glass bell was used as a solvent trap to prevent water evaporation from the hydrogels. To prevent excessive hydrogel squeezing, the gap between plates was adjusted for every hydrogel tested by performing a series of short stress sweep tests ($\nu = 1$ Hz; stress range 1 - 5 Pa) to maximize the elastic modulus up to a constant value was reached. The linear viscoelastic range was determined by means of stress sweep tests consisting in measuring the elastic (G') and viscous (G'') moduli variation with increasing shear stress ($1 \text{ Pa} < \tau < 1000$ Pa) at a frequency, $\nu = 1$ Hz. Mechanical spectra (frequency sweep tests) have been recorded applying a constant stress of 4 Pa in the same experimental conditions.

2.4. Stress relaxation experiments

The viscoelastic properties of agarose hydrogels were determined by stress relaxation experiments. Uniaxial compression of hydrogels (16 mm diameter, 17 mm thickness) was performed using a universal testing machine (Mecmesin Multitest 2.5-i) equipped with a load cell of 100 N and applying a compression speed of 10 mm/min. Stress relaxation tests were performed by applying a constant strain of 15 % for 300 s and tracking the decay of the stress as a function of time.

2.5. Coupling of sulfo-SANPAH to agarose

The coupling of sulfosuccinimidyl 6-(4′-azido-2′-nitrophenylamino)hexanoate (sulfo-SANPAH, catalogue number: BIPA109, Apollo Scientific) to agarose was investigated with modifications as previously described [24,39]. After autoclaving, 4 mL agarose of EP (0.9 % w/V), *Gracilaria* (1 % w/V) and *Gelidium* (1.2 % w/V) dispersed in PBS buffer, pH 7.4, were incubated at 60 °C with stirring. Subsequently, 200 μL of a sulfo-SANPAH solution (4.9 mg/mL, PBS buffer) was added dropwise and the resulting mixtures were immediately irradiated with a UV LED lamp (λ = 365 nm, 35 W, Hobbyland) for 30 min. At the end of the incubation, the mixtures were poured into cylindrical supports to allow them to gel. The hydrogels were washed extensively with deionized water and subjected to freeze-thaw cycles to remove the unreacted sulfo-SANPAH and most of the solvent from the hydrogels. Finally, the resulting hydrogels were dried at 60 °C under vacuum and stored at 4 °C. The success of coupling was verified through UV spectroscopy using a Shimadzu UV-2450 double beam UV/vis spectrophotometer. The spectra were recorded at T = 50 °C.

2.6. Quantification of fibronectin density on the hydrogel surface

Fibronectin was labeled as described in the Supplementary Material section and covalently coupled on the surface of agarose hydrogels using sulfo-SANPAH chemistry (see paragraph 2.9 for complete details). The next day, the hydrogels were washed extensively with PBS and punched to obtain 6 mm diameter disks. They were then placed on a coverslip and analyzed by epifluorescence microscopy using a Plan Fluor 10× DIC L N1 objective. The images were acquired with identical acquisition settings to allow comparison of fluorescence intensities between the analyzed samples and were processed with Fiji-ImageJ. The density of fibronectin was determined as the fluorescence intensity, measuring the intensity of 10 different 10 × 10 μm fields using the ImageJ ROI manager tool. The amount of fibronectin not bound to the surface of the hydrogels was also checked in the wash buffer by a MicroBCA protein assay kit (ThermoFisher); the assay was performed according to the manufacturer's instructions.

2.7. Nanoindendation experiments of hydrogel surface

Indentation experiments of hydrogel surfaces were performed with Chiaro nanoindenter (Optics11 Life, Amsterdam, The Netherlands). The hydrogels were probed using a cantilever-based probe featuring a spherical tip with a radius of 11 µm and a spring constant of 0.45 N/m. Measurements were conducted in indentation control mode, ensuring a constant indentation rate of 10 µm/s throughout the loading phase. Multiple matrix scans were acquired using a 10 µm step size in an x-y plane, resulting in a total of 9 measurement points (arranged in a 3 × 3 grid) per hydrogel. The load-indentation curves obtained from these scans were further analyzed, employing the Hertzian fit model to determine the apparent Young's modulus. Subsequently, the calculated Young's modulus values were utilized to generate 30 × 30 µm heat (force) maps for visualization of the local stiffness of the measured hydrogel area. All measurements were performed at room temperature and in PBS.

Indentation experiments of hydrogel surfaces were also performed by atomic force microscopy (AFM). AFM force-distance curves on the hydrogel samples were acquired on an MFP-3D Bio instrument (Oxford Instruments - Asylum Research) in PBS using pre-calibrated cantilevers with beads from Novascan (diameter 2.5 µm, spring constant 0.06–0.07 N/m). 3 to 4, 6 × 6 force maps, were acquired in different positions for a total of 108 to 144 curves acquired per sample. Only curves with an indentation depth ranging from 100 to 500 nm were considered for the Young's modulus evaluation. Analysis of force-distance curves was performed using AtomicJ after calibration of the sensitivity of the instruments by performing force-distance curves on a glass slide in liquid. The apparent Young's modulus was calculated using a classic Hertzian model using as fixed parameters the radius of curvature of the sphere and the Poisson's ratio (P = 0.5).

2.8. Cell culture

Human osteosarcoma MG63 (ATCC CRL-1427) and human hepatic stellate LX-2 (kindly provided by Prof. Ralf Weiskirchen, Institute of Molecular Pathobiochemistry, Experimental Gene Therapy and Clinical Chemistry, RWTH University Hospital Aachen, Aachen, Germany) cells were cultured in Dulbecco's modified Eagle's Medium High glucose with 0.584 g/L L-glutamine and 0.11 g/L sodium pyruvate (EuroClone, Italy), supplemented with 10 % V/V (in the case of MG63) or 2 % V/V (in the case of LX-2) heat-inactivated fetal bovine serum (Cat. n° ECS0180L, Lot. n° EUS00D4 or Lot. n° EUS00CZ, Euroclone, Italy) and 1 % penicillin/streptomycin (EuroClone, Italy), in a humidified atmosphere of 5 % CO_2 at 37 °C.

2.9. Plating of cells atop hydrogels (substrates)

After autoclaving and temperature curing of agarose, 400 μL of the solutions were distributed into 24-well plates and allowed to rest for 30 min at room temperature to promote gelation. Finally, the hydrogels were incubated overnight at 37 °C in water-saturated conditions. Fibronectin from bovine plasma (Sigma, Product No F1141; UniProt accession no P07589) or the short RGD-peptide described in Supplementary Material were incubated with sulfo-SANPAH (1 mg/mL final concentration) in PBS buffer, pH 7.4, for 4 h at room temperature under dark conditions and shaking. The final concentration of fibronectin and short peptide was 20 μg/mL and 5 mM respectively. Next, 60 μL of the protein/sulfo-SANPAH mixture or PBS, used as control, were added to the hydrogel surfaces and the latter immediately UV-irradiated for 30 min. The hydrogels were washed extensively with PBS (1 rapid washing at room temperature with 1 mL/well followed by 3 long washing steps, 1 mL/well, 30 min each at 37 °C) to discard the unreacted mixture. Cells were finally plated at a density of 20,000 cells/cm^2 with 1.6 mL of cell culture medium/well supplemented with 10 % or 2 % FBS, giving a final V_{PBS}/V_{medium} ratio of 20:80 V/V. Further experiments were carried out with agarose substrates without fibronectin coupling on the surface, to which cells were plated using a cell culture medium without FBS but supplemented with fibronectin (3 or 10 μg/mL) or human vitronectin (5 μg/mL, Advanced Biomatrix, Catalog #5051; UniProt accession no P04004). In all conditions tested, the cells were incubated in a humidified atmosphere with 5 % CO_2 at 37 °C.

2.10. Assessment of cell adhesion

After 24 h or 48 h incubation, cell culture medium was discarded and hydrogels washed with PBS in order to remove non-adherent cells. Then, 500 μL/well of PBS were added and the number of adherent cells/mm^2 and cell spreading area were quantified by Fiji-ImageJ software (multi-point and freehand selection tools, respectively) from images acquired through a Nikon Ti Eclipse inverted bright-field microscope equipped with an Intensilight Epi-fluorescence Illuminator, a Perfect Focus 3 system and a Plan Fluor 10x DIC L N1 objective. Acquisition was performed with a DS-Qi2 16 Mpixel camera (Nikon). Only isolated, *i.e.* non-aggregated cells were analyzed.

2.11. Blocking adhesion experiments

Cells were pre-incubated in suspension for 30 min with the following integrin blocking antibodies: mouse anti-human integrin β_1 monoclonal antibody (dilution 1:100 or 10 μg/mL, clone P5D2, MAB1959, Chemicon); mouse anti-human integrin α_5 monoclonal antibody (dilution 1:100 or 10 μg/mL, clone P1D6, MAB1956Z, Chemicon); mouse anti-human heterodimer $\alpha_v\beta_3$ monoclonal antibody (dilution 1:100 or 10 μg/mL, clone LM609, MAB1976Z, Chemicon). After 30 min, FBS (2 or 10 % V/V) was added and the cells plated on EP-based substrates (20,000 cells/cm^2). Furthermore, cells were plated on EP-based substrates in the presence of 2 % or 10 % V/V FBS and the following chemicals: ML-7 hydrochloride (25 μM, Santa Cruz Biotechnology); cytochalasin D (2 μM, Santa Cruz Biotechnology); PF-562,271 (100 nM, Sigma). The incubation of cells proceeded overnight in a humidified atmosphere of 5 % CO_2 at $T = 37$ °C. The day after they were extensively washed with PBS and the number of cells/mm^2 was determined as described above.

2.12. Statistical analysis and software

Statistical comparisons and graphical elaborations were carried out using GraphPad Prism software. The data distributions were tested for normality using the D'Agostino-Pearson omnibus or the Shapiro–Wilk normality test. Parametric or non-parametric tests were then selected to perform the statistics between the different groups. The specific statistics are reported as indicated in the figure captions. The cartoons were created with BioRender.com.

3. Results

3.1. Bulk mechanical properties of hydrogels from agaroses of different origin

We have developed hydrogels using agaroses with different total content and pattern of methylation as described in Table S2 in the Supplementary Material. Controlled temperature quenching of agarose dispersed in PBS buffer after autoclaving, followed by an equilibrium phase, was used as the experimental approach to form three-dimensional networks [14,16]. Initially, the hydrogels were analyzed under oscillatory mechanical stimulation by rheology. Frequency sweep analyses using a low applied stress - well within the linear viscoelastic range - on agarose hydrogels from electrophoresis (EP), *Gracilaria* and *Gelidium* show a weak dependence of the elastic modulus, G', on the angular frequency, given $(G' \propto \omega^{0.05})_{\omega \to 0}$, and a $G' > G''$ behavior for at least two orders of magnitude of the analyzed angular frequencies (Fig. 1). Experimental points are well fitted by a combination of three Maxwell elements composed by a sequence of "in-parallel" springs and dashpots according to Eqs. (1) and (2) [40,41]

$$G' = G_e + \sum_{i=1}^{3} G_i \frac{\left(\lambda_i\,\omega\right)^2}{1+\left(\lambda_i\,\omega\right)^2}; \quad G_i = \frac{\eta_i}{\lambda_i} \tag{1}$$

$$G'' = \sum_{i=1}^{3} G_i \frac{\lambda_i\,\omega}{1+\left(\lambda_i\,\omega\right)^2}; \quad G_i = \frac{\eta_i}{\lambda_i} \tag{2}$$

where n is the number of Maxwell elements considered, G_i, η_i, and λ_i represent the spring constant, the dashpot viscosity, and the relaxation time of the ith Maxwell element, respectively. G_e is the spring constant of the last Maxwell element which is supposed to be purely elastic. The number of the Maxwell elements was selected based on a statistical procedure to minimize the product $\chi^2 \times N_p$, where χ^2 is the sum of the squared errors, while N_p indicates the number of fitting parameters. The fitting of the experimental data was carried out under the assumption that the relaxation times are not independent of each other, but are scaled by a factor of 10. The sum of spring constants *plus* G_e (Eq. (3)) defines the shear modulus, G, which gives an estimation of the bulk stiffness of the agarose hydrogels:

$$G = G_e + \sum_{i=1}^{3} G_i \tag{3}$$

The calculated shear modulus is ~ 6 kPa for the three sets of hydrogels investigated, indicating the same stiffness for networks of agaroses from different sources (Fig. 1).

Viscoelastic nature of hydrogels from agaroses of different origins was identified extrapolating the loss tangent ($tan\delta$), at $\omega = 6.28$ rad s^{-1} from mechanical spectra and performing stress-relaxation experiments under uniaxial compression. While $tan\delta$ flattens around 5 % indicating a more elastic nature rather than viscous behavior (Supplementary Material, Fig. S4a), stress-relaxation experiments at fixed strain of 15 % indicate a fast decay of applied load [42], with time needed to halve the stress around 60–80 s for all hydrogels investigated (Supplementary Material, Fig. S4b).

Next, strain sweep experiments at fixed angular frequency, *i.e.* $\omega = 6.28$ rad s^{-1}, and increasing strain were undertaken to provide information about the extent of linear stress–strain regime and the onset of non-linear region (Fig. 2). Hydrogels from agaroses of different origin show a linear stress-strain response up to a critical strain where the experimental data deviate from linearity and define a progressive softening of the network due to the irreversible unzipping of the hydrogen bond-based junctions. It is interesting to note how EP agarose hydrogels deviate from linearity at lower strain values compared to *Gracilaria* and *Gelidium*. To provide additional information, the critical strain, γ_c, which marks the onset of the non-linear stress-strain region, is determined modelling the experimental points using Eqs. (4) and (5) [16,18]

$$\sigma = \frac{G_0}{1+b\gamma}\gamma \tag{4}$$

$$\gamma_c: \ \frac{\sigma}{G_0 \cdot \gamma} = 0.95 \tag{5}$$

where G_0 corresponds to the shear modulus at $\gamma_{\to 0}$ and b is a fitting parameter. Examination of the critical strain values shown in Fig. 2 as a function of hydrogels from agaroses of different origin reveals a significant difference between EP, *Gracilaria* and *Gelidium* networks, suggesting that EP begins to soften at lower strain. Taking the mechanical results together, we conclude that hydrogels from agaroses of different origin have the same bulk stiffness and very similar viscoelasticity but a different ability to break under strain.

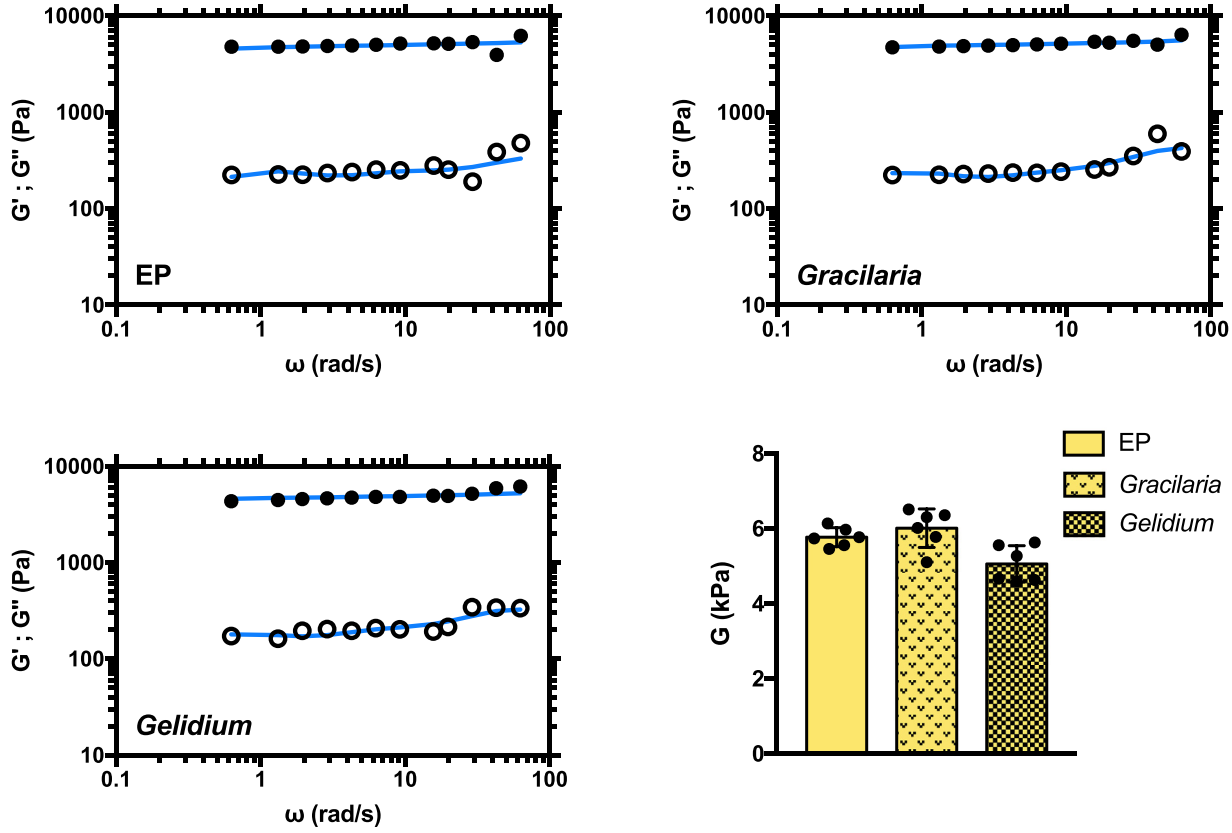

Fig. 1. Mechanical spectra and determination of the bulk stiffness for hydrogels from agaroses of different origin. The solid black dots represent the experimental values of the elastic modulus, G', while the empty the viscous modulus, G''. The light blue solid lines represent the fit by Eqs. (1) and 2. In the bar chart is reported the shear modulus, G, calculated according to Eq. (3), which gives an estimation of the hydrogels stiffness; data are reported as mean ± s.d., $n = 6$ hydrogels analyzed for each experimental condition. Frequency sweep measurements were performed with a constant stress of 4 Pa and $T = 37$ °C. Composition of hydrogels: [EP] = 0.9 % w/V, [*Gracilaria*] = 1 % w/V, [*Gelidium*] = 1.2 %; PBS buffer, pH 7.4.

3.2. Coupling of RGD-containing fibronectin and evaluation of the nanomechanical properties of the hydrogel surface

Next, we coupled RGD-containing fibronectin to the surface of agarose hydrogels using the hetero-bifunctional crosslinker sulfo-SANPAH [24,39]. First, we verified the chemical coupling of pure sulfo-SANPAH to agarose by UV spectroscopy. Sulfo-SANPAH dispersed in deionized water shows an absorption peak at 262 nm, corresponding to the photoactive nitrophenyl azide group, and a spectrum profile comparable to that reported elsewhere (Supplementary Material, Fig. S5) [43]. When sulfo-SANPAH is mixed with agaroses in PBS buffer, pH 7.4, and irradiated with UV light, the nitrene group of bifunctional cross-linker is activated and initiates coupling. Covalent grafting to agarose backbone is confirmed by the presence of a similar absorbance peak, shifted at ∼ 280 nm (Fig. 3a), probably due to the different electronic environment caused by the chemical modification at the aromatic ring.

Bovine fibronectin containing two RGD motifs in positions 1616–1618 and 2183–2185 is first incubated with sulfo-SANPAH under dark conditions to favor the reaction between the primary amines of the protein and the sulfo-NHS group of the crosslinker, then deposited atop the surface of the hydrogels and finally irradiated with UV, as shown in the cartoon in Fig. 3b. Fluorescent microscopy images of the surface of the hydrogel show an almost uniform distribution of fibronectin (Fig. 3c). Quantification of 10 × 10 μm ROI areas reveals a protein fluorescence density that is significantly dependent on agarose type, with the highest observed in the case of *Gelidium* (Fig. 3d). This was confirmed by the quantification of uncoupled fibronectin in the supernatants discarded after washing by micro BCA assay (Fig. 3e), showing the exact opposite trend with respect to the protein density reported in Fig. 3d. Both results indicate that EP-based hydrogels contain less fibronectin on the surface, while the *Gelidium*-based counterparts contain the highest amount.

Next, we wondered whether fibronectin coupling would affect the nanomechanical properties of the hydrogel surface. The Chiaro nanoindenter was used to probe the surface of the hydrogels. The 30 × 30 μm scans indicate different force maps depending on the agarose type and chemical functionalization (Fig. 3f). Interestingly, the Young's modulus significantly decreases when switching from non-functionalized EP- to *Gelidium*-based hydrogels (Fig. 3g). This is also confirmed when examining the same surfaces by atomic force microscopy (Supplementary Material, Fig. S6). When fibronectin is coupled *via* sulfo-SANPAH chemistry, the same trend is not maintained, although the surface of *Gelidium*-RGD hydrogels is significantly softer compared to EP-RGD and *Gracilaria*-RGD hydrogels. Importantly, when comparing non-functionalized with functionalized hydrogels, the coupling of RGD-containing fibronectin has no effect on the Young's modulus of hydrogels from agaroses of different origin (Fig. 3g and Table S3 in Supplementary Material for a complete overview of the statistics).

3.3. Coupled adhesive peptide sequences enhances cell adhesion or not, depending on substrate type, fetal bovine serum content and peptide structure

Hydrogels from agaroses of different origin were next tested as 2D substrates for cell adhesion. First, the human osteosarcoma cell line MG63 was plated on fibronectin-functionalized substrates in

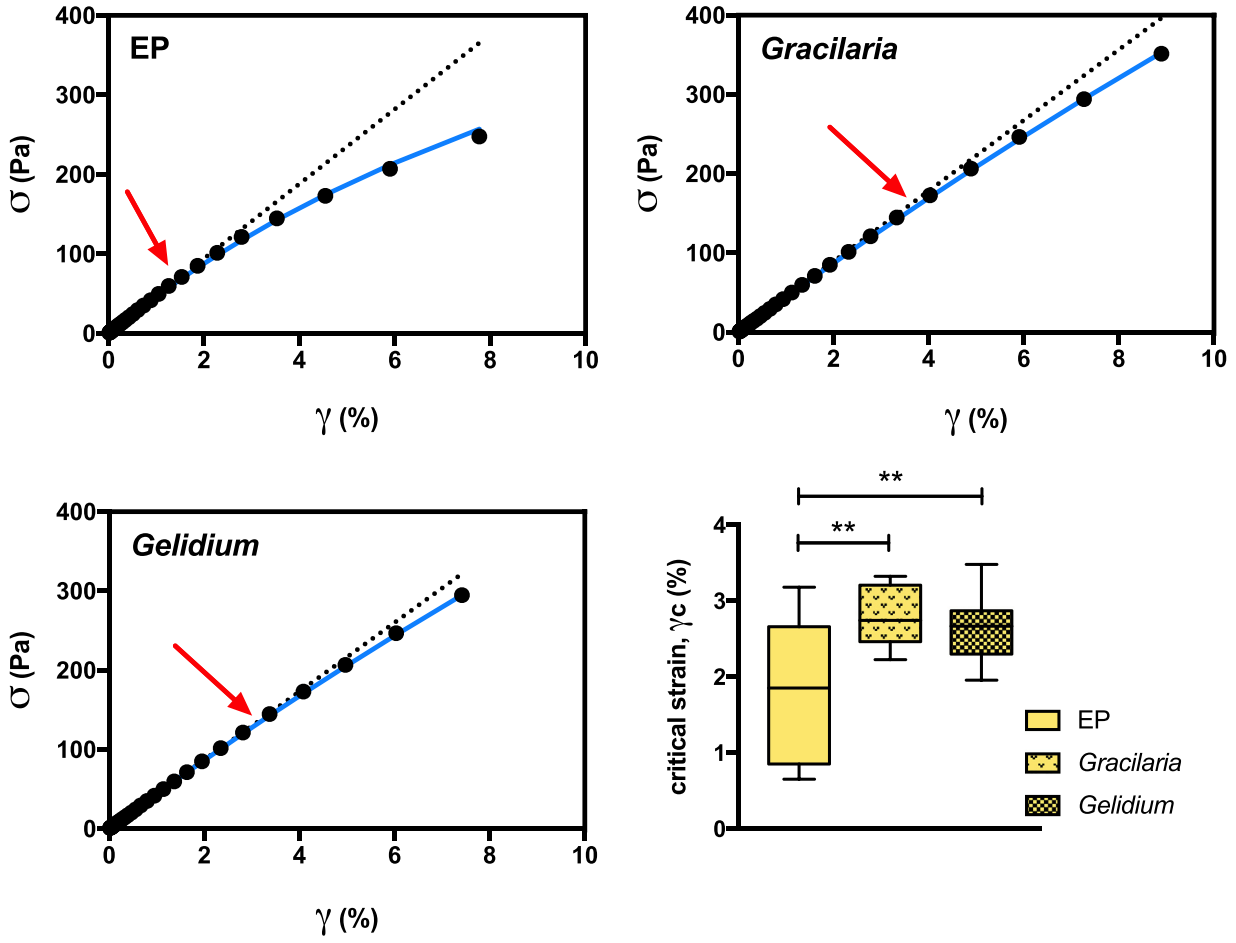

Fig. 2. Hydrogels from agaroses of different origin break differently under strain. Stress–strain curve profiles of hydrogels from agaroses of different origin. Black dots are the experimental points, while the light blue solid lines represent the fit by Eq. (4). The dotted black line is the theoretical linear stress–strain response of the hydrogels up to the deformation investigated. The red arrows indicate the onset of non-linear (softening) region. In the box and whiskers chart is reported the critical strain, γ_c, calculated according to Eq. (5), which indicates the onset of softening region; data are reported from min to max, n = 10 - 15 hydrogels analyzed for each experimental condition. Stress sweep measurements were performed with a constant angular frequency of 6.28 rad s^{-1} and T = 37 °C. Composition of hydrogels: [EP] = 0.9 % w/V, [*Gracilaria*] = 1 % w/V, [*Gelidium*] = 1.2 %; PBS buffer, pH 7.4. Statistics: **, $p < 0.01$; One-way ANOVA followed by Dunnett's Multiple Comparisons test.

the presence of a low FBS content, *i.e.* 2 % V/V, in the cell culture medium. Under these experimental conditions, the RGD-containing fibronectin sequence significantly improves the number of cells attaching to the EP agarose-based hydrogels and cell spreading area (Fig. 4, top panel and Fig. S7 in Supplementary Material). Nonetheless, limited spheroid-like aggregates can also be seen without RGD motif. However, in the case of *Gracilaria* and *Gelidium*, the presence of covalently coupled fibronectin is not helpful for cell attachment. In this case, the MG63 prefer to interact with each other and form spherical aggregates with different sizes depending on agarose type. This is confirmed when human hepatic stellate LX-2 is used as a second cell model (Supplementary Material, Fig. S8). Again, the EP-RGD substrate supports cell adhesion, which is significantly improved compared to the RGD-free counterpart. In LX-2, it is noticeable that the presence of RGD enables the adhesion of a very limited number of cells atop both *Gracilaria* and *Gelidium*. Interestingly, when a short oligopeptide containing the RGD sequence is coupled to the agarose hydrogels instead of fibronectin, the enhancement of cell adhesion in EP hydrogels is not observed, suggesting a structure-function relationship between the presentation of peptide adhesive sequences and cell anchoring (Supplementary Material, Fig. S9). Nonetheless, the enhancement in cell adhesion on EP-RGD substrates is fully or partially suppressed when using myosin light chain kinase, focal adhesion kinase inhibitors and the blocking antibody against α_5 integrin (Supplementary Material, Fig. S10).

When the FBS in the cell culture medium is increased to 10% V/V, which corresponds to the usual conditions for cell cultures, an interesting scenario emerges. The surface-coupled fibronectin does not improve the number of cells/mm^2 on EP-RGD substrates, but only slightly increases cell spreading and formation of stress fibers (Fig. 4, lower panel and Fig. S7 and 11 in Supplementary Material), suggesting that cell adhesion is dependent on adsorbed proteins of FBS rather than coupled fibronectin. Again, cell adhesion is strongly inhibited on *Gracilaria* and *Gelidium* substrates, although the amount of adsorbed proteins from FBS is similar compared to EP substrates (Supplementary Material, Figure S2), and the coupling of RGD-containing fibronectin is not beneficial. A significant reduction in cell adhesion on EP-RGD substrates is observed when intracellular tension, focal adhesion kinase (FAK) activity and the heterodimer $\alpha_v\beta_3$ integrin are perturbed (Supplementary Material, Fig. S12). Overall, these results show that coupled RGD-containing fibronectin enhances cell adhesion mostly under low FBS conditions. This clearly depends on substrate type, peptide structure and requires intracellular tension, functionality of FAK and the engagement of either α_5 integrin or the heterodimer $\alpha_v\beta_3$ depending on the amount FBS in the cell culture medium.

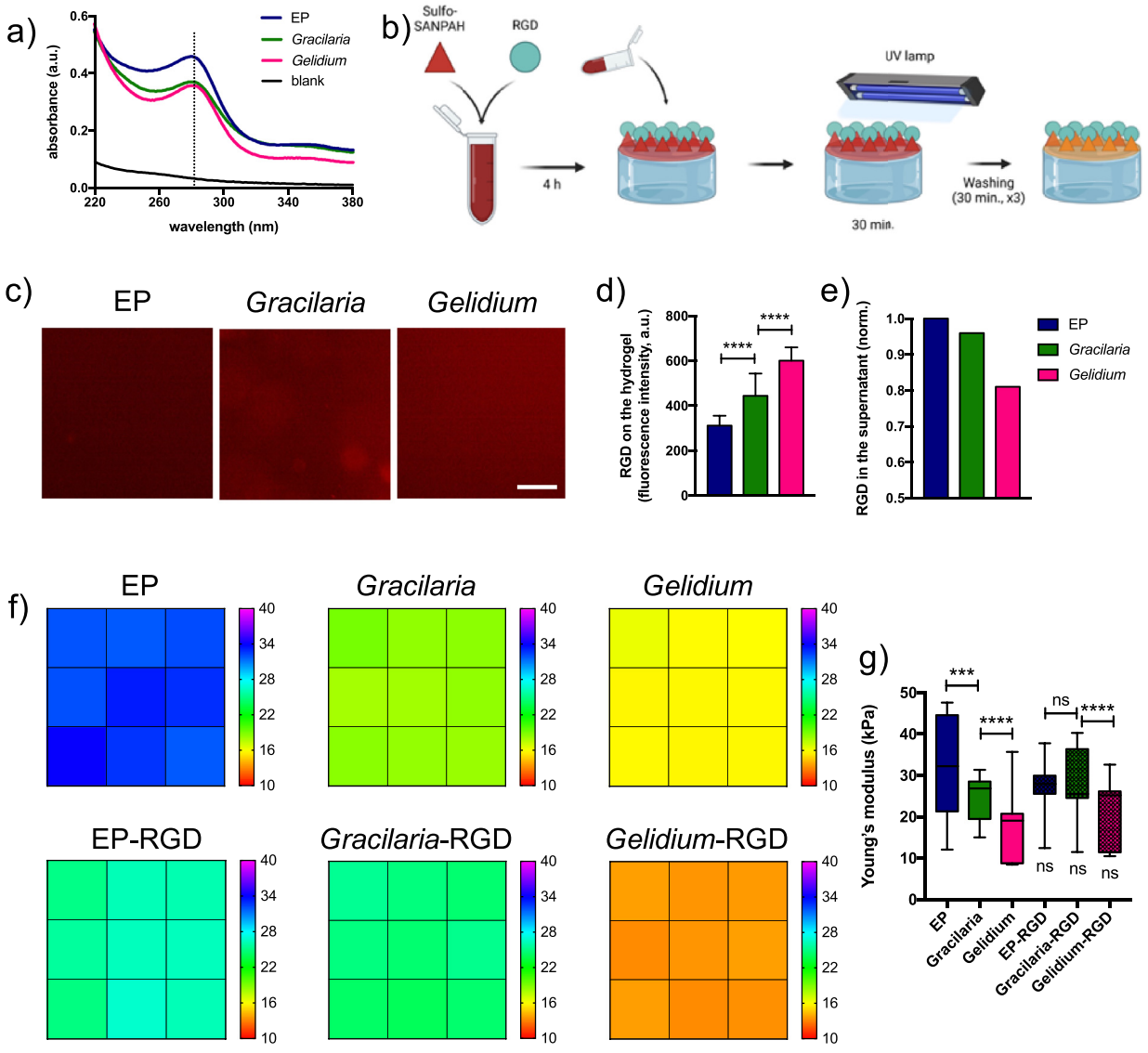

Fig. 3. The coupling of fibronectin depends on the agarose type and does not reduce the Young's modulus of hydrogel surfaces. **(a)** UV spectra of agaroses from different origin when coupled with sulfo-SANPAH; the blank sample represents an agarose sample as reference without the cross-linker; the dotted line indicates the absorbance peak at around 280 nm; the spectra were recorded at $T = 50$ °C and using deionized water as solvent. **(b)** Schematics of the experimental protocol used in this study to graft the RGD-containing fibronectin on the agarose hydrogels surface. **(c)** 450 × 450 μm fields from fluorescent microscopy analysis and **(d)** fluorescence intensity of RGD-containing fibronectin quantified on the hydrogels surface by measuring the intensity of 10 μm × 10 μm fields using the ImageJ ROI manager tool; the scale bar in (c) is 100 μm; data in (d) are reported as mean ± s.d., $n = 89$; statistics: ****, $p < 0.0001$; One-way ANOVA followed by Tukey's Multiple Comparisons test. **(e)** Quantification of fibronectin in the washing buffer through micro BCA assay; the data are reported as the mean of two independent determinations. **(f)** 30 × 30 μm heat (force) maps from Chiaro nanoindentation experiments; each cell in the map is 10 μm wide in an x-y plane; the color bars indicate the Young's moduli in the range 10 - 40 kPa. **(g)** Apparent Young's moduli of the hydrogel surfaces; experimental data are reported as box and whiskers (min to max), $n = 127 - 152$; statistics above box and whiskers are between different types of hydrogels, while those below refer to changes from surface coupling of fibronectin of the same hydrogel type: ns, not significant; ***, $p < 0.001$; ****, $p < 0.0001$; Kruskal–Wallis test followed by Dunn's Multiple Comparisons test. For a complete overview of the statistics in (g) see Table S3 in the Supplementary Material.

3.4. Cell adhesion to EP substrates is mediated by $\alpha_v\beta_3$ integrin and requires vitronectin in FBS, actomyosin contractility and FAK activity

Next, we performed experiments to investigate the role of FBS in cell adhesion using EP substrate (hence without coupled RGD-containing fibronectin) as model. FBS is a heterogeneous mixture of cell-adhesive (fibronectin and vitronectin) and non-adhesive (albumin, which is the most abundant) proteins with batch-to-batch variability [31–33]. Liquid chromatography with tandem mass spectrometry confirmed the presence of fibronectin and vitronectin in the FBS in a ratio of 1:5 (Supplementary Material, Fig. S1). Firstly, we checked whether the anchoring of the cells is mediated by the fibronectin contained in the FBS. Cells bind to the RGD and the "synergy" PHSRN peptide sites in fibronectin via the heterodimer $\alpha_5\beta_1$ integrin and require mechanical tension of myosin-actin axis [44]. Thus, MG63 were pre-incubated with α_5 (highly specific for fibronectin) and β_1 (less specific for fibronectin) blocking antibodies and then plated in the presence of 10% V/V serum (Fig. 5a). The results show that the cells adhere and spread even in the presence of blocking antibodies, suggesting that fibronectin in FBS does not play a significant role in anchoring the cells to the EP substrate via the $\alpha_5\beta_1$ heterodimer. This is confirmed by a control experiment in which the cells are plated using a serum-free cell culture medium but supplemented with an increasing amount of fibronectin (Supplementary Material, Fig. S13). We have also ruled out the possibility that non-adhesive proteins such as BSA contribute to exposing the hidden adhesive synergy site in fibronectin, thereby promoting cell adhesion via $\alpha_5\beta_1$ heterodimer (Supple-

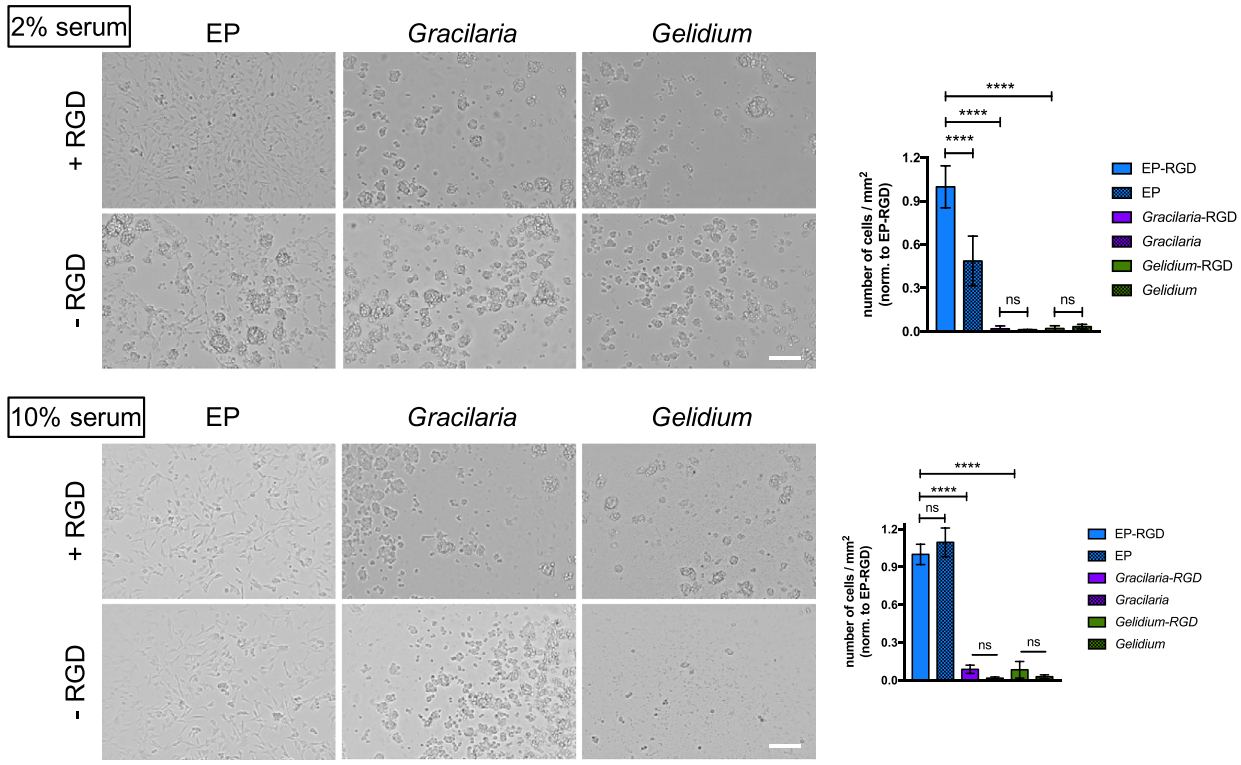

Fig. 4. RGD-containing fibronectin coupling on the surface of agarose hydrogels improves cell adhesion depending on the agarose type and under culture conditions with low serum content. Representative images of MG63 cells adhered to hydrogels of agarose of different origin in the presence of 2% V/V (upper panel) or 10% V/V (lower panel) fetal bovine serum in cell culture medium. RGD (fibronectin)-coupled substrates are compared with the same hydrogels without coupled fibronectin; scale bars are 200 μm. The images were taken after 48 h of cell seeding. The bar charts represent the total cell number/substrate area; data are displayed as normalized to EP-RGD sample, and reported as mean ± *s*.d., n = 6–18 images analyzed for EP case, n = 2 - 15 for *Gracilaria* and n = 3–15 for *Gelidium*. Statistics: ****, $p < 0.0001$; ns, not significant; One-way ANOVA followed by Tukey's Multiple Comparisons test.

mentary Material, Fig. S14) [36]. As expected, however, the cells anchor the substrate if the fibronectin was previously applied to the substrate as a coating (Supplementary Material, Fig. S15) [30].

Secondly, we tested whether the anchoring of the cells is mediated by the vitronectin contained in the FBS. Vitronectin has an RGD site that can be recognized by the heterodimer $\alpha_v\beta_3$ integrin expressed by osteosarcoma cells such as MG63 [45,46]. Therefore, the cells were pre-incubated with the $\alpha_v\beta_3$ blocking antibody and then plated in the presence of serum. In this case, a dramatic reduction in cell number/surface area is observed (Fig. 5b). The combination of $\alpha_v\beta_3$ + α_5 blocking antibodies does not reduce further cell adhesion, confirming that the anchoring is dependent on the $\alpha_v\beta_3$ rather than $\alpha_5\beta_1$ integrin type. The chemical inhibition of myosin light chain kinase, actin polymerization and FAK activity demonstrates the importance of intracellular mechanical tension and the activity of the myosin-actin-integrin axis for anchoring the cells to the EP substrate by the help of FBS (Fig. 5c). From a macromolecular point of view, the RGD motif of vitronectin is partially cryptic and the protein exhibits a high degree of conformational flexibility [47,48]. When treated by heating, chaotropic agents, acidification or complexation with specific proteins vitronectin can multimerize [49]. In our experiments, we heat FBS at 56 °C to destroy the functional activity of complement and other factors before supplementing the cell culture media. We therefore wondered whether heating would lead to a conformational change of vitronectin with a possible differential exposure of the RGD sequence. To test this, we plated MG63 with cell culture medium supplemented with heat-treated or non-heat-treated FBS. Similarly, we performed the same experiments with a cell culture medium supplemented with the only vitronectin (Fig. 5d). Remarkably, in both cases, heat treatment leads to a significant reduction in cell number/surface area, suggesting that heat treatment of proteins reduces the ability of the cells to recognize the RGD motif and consequently to anchor the substrate. Taken together, we conclude that cell adhesion to EP substrates is mediated by $\alpha_v\beta_3$ integrin-RGD motif of vitronectin contained in FBS and requires intracellular mechanical tension due to the functionality of the myosin-actin-integrin machinery.

4. Discussion

The basis of this study is the unexpected evidence that agarose can become a compliant 2D substrate for cell culturing under certain experimental conditions without the use of previously coupled or adsorbed specific adhesive peptide sequences [16,18,30]. In our earlier studies, we demonstrated that agarose hydrogels must fracture easily under oscillatory shear to achieve this. That is, the shorter the linear stress–strain response of the hydrogel and thus the easier the entry into the nonlinear (plastic) region, the stronger the adhesion and spreading of cells, the transduction of biophysical cues and the transmission of forces to the substrate. Beside mechanics, we have found that fetal bovine serum present in cell culture medium plays a key role as protein reservoir to promote cell anchoring to the substrate.

To elucidate the relationship between substrate mechanics, the FBS used in standard cell culture media and specific cell-adhesive peptide sequences that promote adhesion to the network, we have exploited agarose hydrogels exhibiting same bulk stiffness and very similar viscoelasticity but different critical strain at which linear stress-strain regime ends (Figs. 1 and 2 and Fig. S4 in the Supplementary Material). The surface of these materials can be decorated with the cell-adhesive RGD motifs using sulfo-SANPAH chemistry

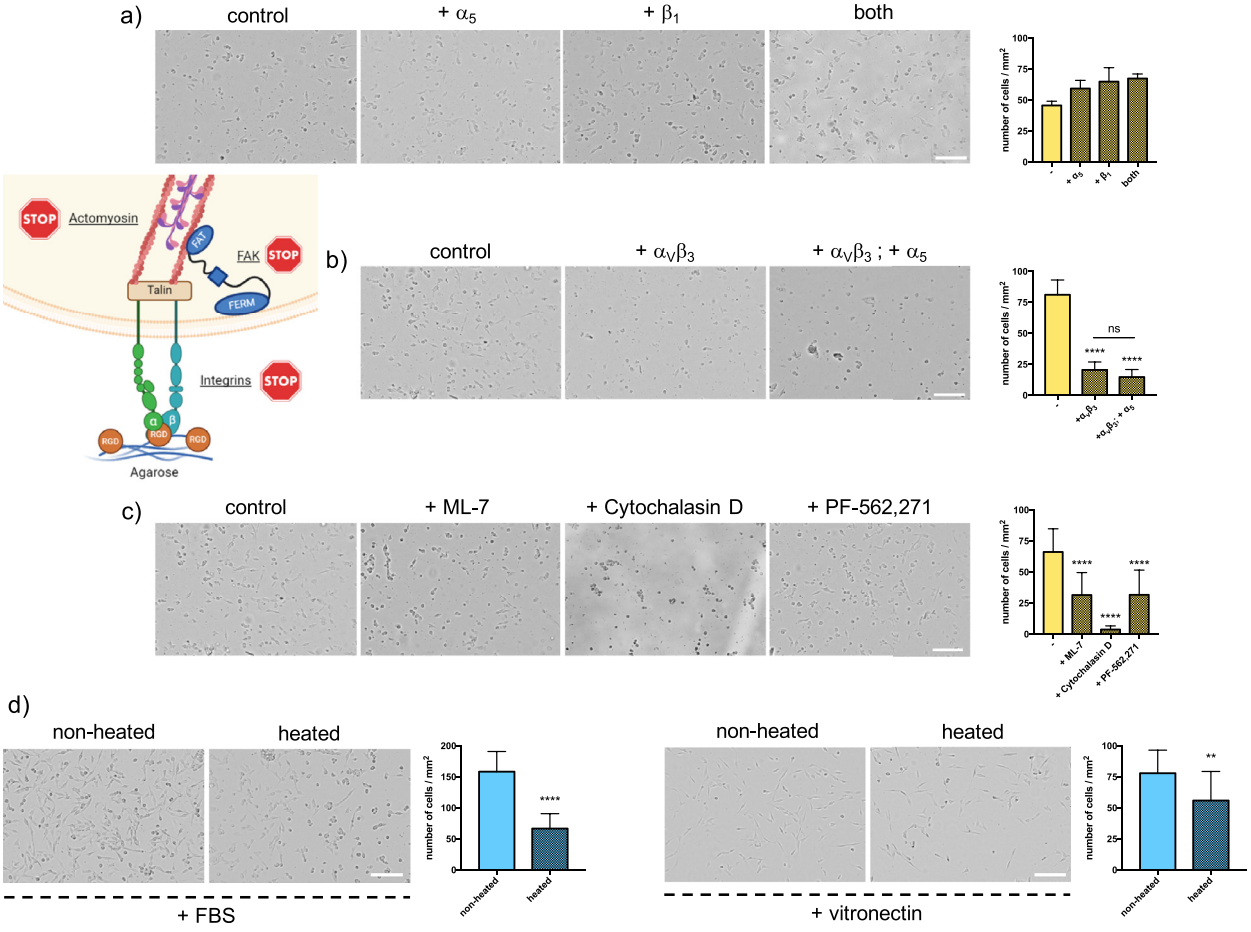

Fig. 5. Cell adhesion to EP substrate exploiting FBS as protein reservoir is mediated by $\alpha_v\beta_3$ and not by $\alpha_5\beta_1$ heterodimer, and requires vitronectin as RGD supplier, actomyosin contractility and FAK activity. Representative images of MG63 cells adhered to EP-based hydrogels in the presence of α_5 and β_1 blocking antibodies **(a)**, $\alpha_v\beta_3$ and α_5 blocking antibodies **(b)**, and inhibitors of actomyosin contractility and FAK activity **(c)**. The cartoon on the left displays the specific points at which actomyosin-integrin axis and FAK are blocked. In the case of blocking antibodies, the cells were pre-incubated for 30 min with the antibodies and then supplemented with 10% V/V fetal bovine serum in cell culture medium; scale bars are 200 μm in all images. **(d)** Representative images and quantification of MG63 cells adhered to EP-based hydrogels plated with cell culture medium supplemented with heated or non-heated 10% V/V FBS or vitronectin (5 μg/mL). In all experiments the images were taken after 24 h of cell seeding. The bar charts represent the total cell number/substrate area; data are displayed as mean ± s.d., n = 5 images analyzed in (a), n = 5 - 16 in (b), n = 10 - 28 in (c) and n = 17 - 18 in (d). Statistics: **, $p < 0.01$; ****, $p < 0.0001$; ns, not significant; One-way ANOVA followed by Dunnett's Multiple Comparisons test with respect to control group in (a-c) and unpaired two-tailed t-test in (d).

as previously described [24,39]. Interestingly, we found a correlation between the amount (density) of RGD-containing fibronectin introduced by the coupling process and the agarose type (Fig. 3d). The mechanism of coupling of sulfo-SANPAH to a polysaccharide backbone was investigated in the case of chitosan and revealed that the nitrene group of sulfo-SANPAH inserts into the -OH group at the C_6 position of the polysaccharide unit [50]. Remarkably, we can observe an inverse correlation between the methylation degree at the same C_6 position of the galactose moiety and the amount of coupled fibronectin on the surface of the corresponding hydrogels (see Table S2 in Supplementary Material and Fig. 3d). We therefore speculate that the higher the degree of methylation at the C_6 position of the galactose - *i.e.* the lower availability of hydroxyl groups - the lower the fibronectin coupling on the hydrogel surface, leading to EP < *Gracilaria* < *Gelidium* trend as indicated in Fig. 3d.

When cells are plated on this set of substrates, we found that the coupled fibronectin enhances cell adhesion when the FBS concentration in cell culture medium is low, and this particularly depends on the agarose type composing the substrate under consideration (Fig. 4). We have demonstrated this using bovine fibronectin and two cell models, namely human osteosarcoma MG63 and human hepatic stellate cells LX-2. However, the enhancement in cell adhesion only applies to the case of EP-based substrates, which are mechanically compliant for cell adhesion [18,30]. In contrast, only very limited cell adhesion is observed when using fibronectin-coupled substrates from *Gracilaria* and *Gelidium* agaroses, confirming again the central role of substrate mechanics in terms of the extent of linear stress-strain response of the network bulk. In 2% V/V FBS conditions, the enhancement of cell adhesion on fibronectin-coupled EP substrates is abolished at a different extent when using myosin light chain kinase, focal adhesion kinase inhibitors and the α_5 blocking antibody (Supplementary Material, Fig. S10), suggesting that cells must exhibit intracellular tension, together with FAK activation and integrin engagement to boost the adhesion. It has already been shown that the role of intracellular tension and mechanoactivation of FAK is to unfold the fibronectin previously coupled to the hydrogel substrate in order to expose its hidden "synergy" site, PHSRN, that can be accessed by α_5 integrin [44]. This site, in combination with the downstream RGD motif recognized by β_1 integrin, would promote a ~100-fold increase in cell adhesion to fibronectin via the engaged $\alpha_5\beta_1$ heterodimer [51]. The fibronectin used in our experiments exhibits the "synergy" sequence in positions 1499–1503, that is highly conserved in bovine (PPSRN) [51], together with the downstream RGD consensus sequence in position 1616. Hence, we conclude that the enhancement of cell adhesion in low FBS condi-

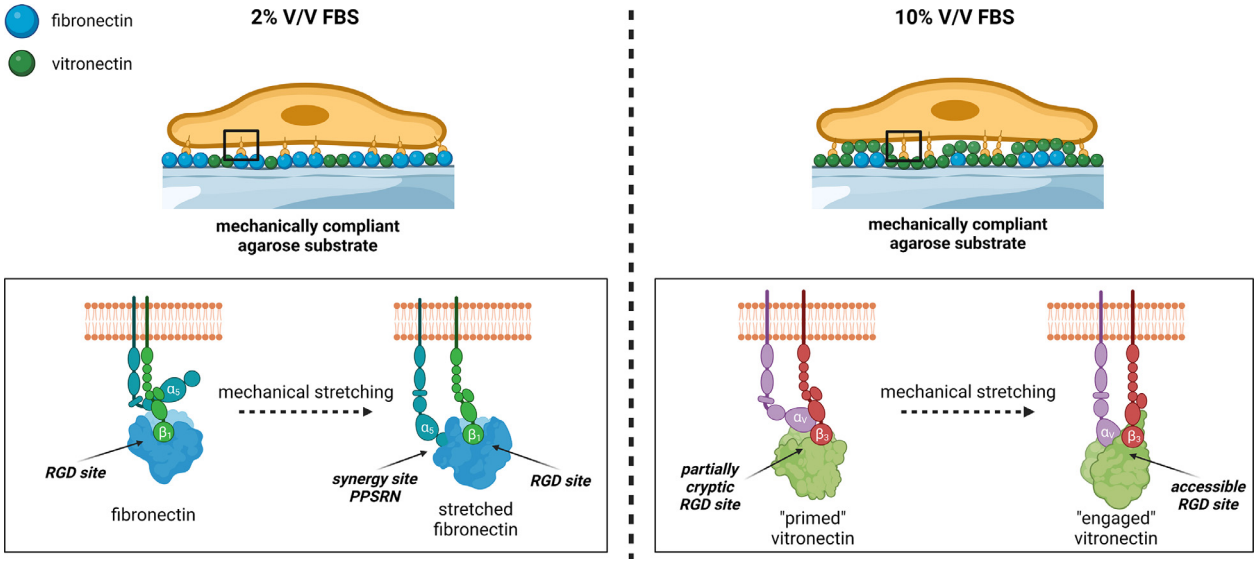

Fig. 6. Elucidating the unexpected cell adhesive properties of agarose substrates. The effect of mechanics, fetal bovine serum and specific peptide sequences. Cartoon summarizing what was identified in this study. The left panel recapitulates the experimental condition in which cells are plated on agarose substrates in the presence of 2% V/V fetal bovine serum (FBS). Here, the cells recognize the coupled fibronectin on the surface of agarose substrate, which enhances cell adhesion; in this context, the amount of vitronectin is low, so it would only plays a marginal role in promoting cell anchoring. The cells recognize both the synergy and RGD sites of fibronectin via $\alpha_5\beta_1$ integrin, stretching the protein and allowing firm cell adhesion and spreading. The right panel recapitulates the experimental condition in which the cells are plated on agarose substrates in the presence of 10% V/V FBS. Here, the serum proteins conceal the coupled fibronectin and the cells respond to them. In particular, vitronectin is identified as the key modulator of FBS that controls cell adhesion via its partially cryptic RGD site, which can be recognized by $\alpha_v\beta_3$ integrin. Thanks to actomyosin contractility, cells stretch the adsorbed vitronectin, the latter switching from a "primed" to an "engaged" state characterized by complete binding of the heterodimer with subsequent cell adhesion and spreading. The model applies to agarose substrates that exhibit short linear stress-strain response of the bulk network under oscillatory shear, such as the EP substrates in this study. It does not apply to more elastic substrates such as those based on *Gracilaria* or *Gelidium*, where neither the coupling of specific peptide adhesive sequences nor the use of 10% V/V FBS helps to restore cell adhesion.

tions observed with EP-RGD substrates is due to a similar mechanism (Cartoon in Fig. 6). This is further supported by the fact that we do not observe the enhancement when we couple an oligopeptide that lacks the synergy site and contains only the RGD motif (Supplementary Material, Fig. S9).

When 10% V/V FBS is used in the cell culture medium, the positive effect of coupled fibronectin on EP substrates mostly disappears (Fig. 4). We found the same number of cells attached to both EP-RGD and EP substrates and showed a very similar morphology in terms of spreading (Supplementary Material, Fig. S7). In these experimental conditions, it is very likely that proteins in the FBS conceal the coupled RGD, so that cell adhesion is mediated by serum proteins. To this, in our previous paper, we have already shown that the serum albumin, which is the major component of FBS, is well adsorbed within 8 μm-depth from the hydrogel surface regardless of agarose type [18]. In this work, we quantified the adsorption of total proteins from FBS under 10% V/V FBS conditions as $\sim$10 μg protein / mg agarose for the case of the EP hydrogel (Supplementary Material, Fig. S2). In addition, we have shown that cell adhesion is impaired on both fibronectin functionalized and non-functionalized substrates when the heterodimer $\alpha_v\beta_3$, *i.e.* the "vitronectin receptor", is blocked prior to incubation of the cells with FBS-containing cell culture medium (Fig. 5 and Figure S12 in Supplementary Material). This does not hold if we block the heterodimer $\alpha_5\beta_1$ (the main fibronectin receptor), suggesting that cell adhesion is mediated by vitronectin rather than fibronectin contained in FBS. This is confirmed by the results reported in Fig. 5d and corroborated by various control experiments (Supplementary Material, Figs. S13,14). Curiously, vitronectin works properly as an adhesive protein when added in solution to the cell culture medium whereas fibronectin does not. The latter restores its adhesive properties when applied as a coating to the EP substrate before cell seeding (Supplementary Material, Fig. S15). This suggests a different binding mode between the synergy and RGD adhesive sequences in fibronectin and the $\alpha_5\beta_1$ heterodimer in the two experimental settings. Indeed, the $\alpha_5\beta_1$ heterodimer switches between a relaxed and a tensioned state in response to intracellular tension [52]. While the relaxed state can only be engaged by the RGD motif, the tensioned state also requires the participation of the synergy site. Thus, when fibronectin is added to the cell culture medium, the cells in suspension - a state in which no intracellular tension is expected - are able to recognize the consensus sequence RGD via the β_1 integrin subtype, but not the synergy via the α_5 integrin subtype. In this state, no intracellular transduction is expected and this has been associated with no FAK activation [44], and, in this study, no cell adhesion to EP substrate (Supplementary Material, Fig. S13). These considerations are strengthened when Vroman effects are taken into account with regard to the different molecular weight and thus the mobility of the two proteins in FBS. Vitronectin and fibronectin are 75 kDa and 220 kDa proteins, respectively. This means that vitronectin has a higher mobility and is likely to be adsorbed faster atop hydrogels and thus can efficiently act as an anchoring point for cells. In contrast, fibronectin is adsorbed more slowly and would therefore justify recognition in suspension by cells, as described above, before it is adsorbed. However, when fibronectin is deposited as a coating, a conformational change of the protein occurs at a concentration $\geq$ 1.25 μg/mL [36], possibly making the synergy site more accessible to the α_5 integrin subtype and thus promoting cell adhesion to EP substrates (Supplementary Material, Fig. S15). Of note, we have demonstrated that actomyosin contractility together with FAK activity are of pivotal importance for cell adhesion mediated by vitronectin (Fig. 5c and Fig. S12 in Supplementary Material). Considering all these results and the fact that vitronectin has a partially cryptic RGD site [47,48], we conclude that: (*i*) the vitronectin contained in FBS and adsorbed on the surface of agarose network behaves like a nascent anchoring point for cells, possibly involving only a subtype of integrin, likewise what happens in fibronectin,

and thus determines a "primed state"; (*ii*) thanks to the onset of intracellular tension generated by actomyosin contractility, the entrapped vitronectin is stretched and the sequence consensus RGD becomes fully accessible to the heterodimer $\alpha_v\beta_3$ determining an "engaged state", which leads to mechanoactivation of FAK, firm cell adhesion and spreading (Cartoon in Fig. 6). This model envisages that vitronectin is first adsorbed on the surface of the EP substrate and then recognized by the cells. However, we cannot exclude partial interactions between the RGD of vitronectin and the heterodimer $\alpha_v\beta_3$, which could occur when the cells are in suspension. Further experiments are required to exclude or confirm this.

5. Conclusions

To summarize, this study elucidates how agarose-based hydrogels can behave as permissive substrates for cell adhesion, challenging the current view which considers this type of biomaterials as non-permissive substrates. On the one hand, the results reported in this work reconcile our previous observations. Namely, they show that a shorter linear stress-strain response of the bulk network under oscillatory shear with subsequent softening is key for cell anchoring and turns agarose-based substrates from non-permissive to permissive. In addition to mechanics, peptide adhesion sequences, particularly RGD motifs, are also necessary for anchoring. Importantly, we have shown that these adhesion sequences can be recognized by cells when they are chemically coupled or physically adsorbed on the surface of agarose substrates. On the other hand, this study would focus on the role of fetal bovine serum in promoting cell adhesion atop hydrogel-based substrates. Here, for example, we have shown that when using 10% V/V FBS in cell culture medium, a standard experimental condition for cell culture, cells respond mostly to the RGD of vitronectin contained in FBS rather than to the synergy and RGD sequences of coupled fibronectin. This would interfere with the response of the cells to specific peptide motifs. Special care should also be taken when using heated or non-heated FBS, as we have observed differences in cell number/surface area that are most likely due to the different 3D configuration of vitronectin and thus the availability of RGD motifs. This is a very interesting point that requires further investigation. Taken together, these results will have a major impact on mechanobiology research.

Declaration of competing interest

The authors declare that they have no known competing financial interests or personal relationships that could have appeared to influence the work reported in this paper.

CRediT authorship contribution statement

Francesco Piazza: Writing – review & editing, Software, Investigation, Data curation, Conceptualization. **Beatrice Ravaglia:** Writing – review & editing, Investigation, Data curation. **Andrea Caporale:** Writing – review & editing, Methodology, Investigation, Data curation. **Ana Svetić:** Writing – review & editing, Methodology, Investigation, Data curation. **Pietro Parisse:** Writing – review & editing, Software, Methodology, Investigation, Data curation. **Fioretta Asaro:** Writing – review & editing, Methodology, Investigation, Data curation. **Gabriele Grassi:** Writing – review & editing, Methodology, Data curation. **Luca Secco:** Writing – review & editing, Methodology, Investigation, Data curation. **Riccardo Sgarra:** Writing – review & editing, Methodology, Investigation, Data curation. **Eleonora Marsich:** Writing – review & editing, Methodology, Conceptualization. **Ivan Donati:** Writing – review & editing, Supervision, Project administration, Methodology, Conceptualization. **Pasquale Sacco:** Writing – review & editing, Writing – original draft, Supervision, Project administration, Methodology, Funding acquisition, Data curation, Conceptualization.

Acknowledgments

This study was supported by the grant D40-microgrants23_SACCO. The images reported in this article were generated in the Light Microscopy Imaging Center of the University of Trieste at the Department of Life Sciences. The proteomics analysis was carried out with the mass spectrometry platform realized thanks to the "Special call for funding the purchase of scientific equipment - Year 2022" of the University of Trieste. P. Sacco gratefully acknowledges the support of CSGI (Consorzio Interuniversitario per lo Sviluppo dei Sistemi a Grande Interfase). We would like to thank the Antimicrobial Peptides Synthesis Lab at the University of Trieste and Prof. Alessandro Tossi. We would like to thank Mrs Sara Lipari for her help with the experimental work. G. Grassi wishes to thank the Italian Ministry of Foreign Affairs and International Cooperation (project VN21GR01). We would like to thank Prof. Ralf Weiskirchen (Institute of Molecular Pathobiochemistry, Experimental Gene Therapy and Clinical Chemistry, RWTH University Hospital Aachen, Aachen, Germany) for providing LX-2 cells. We would like to thank Dr. Loredana Casalis for the useful discussion on AFM and nanoindenation measurements and for the access to the facilities obtained through the project "Pathogen Readiness Platform for CERIC-ERIC Upgrade" PRP@CERIC (PNRR Piano Nazionale di Ripresa e Resilienza, Missione 4 "Istruzione e Ricerca", Componente 2 "Dalla Ricerca all'Impresa", Linea di Investimento 3.1 "Fondo per la realizzazione di un sistema integrato di infrastrutture di ricerca e innovazione", finanziato dall'Unione Europea – Next Generation EU).

Supplementary materials

Supplementary material associated with this article can be found, in the online version, at doi:10.1016/j.actbio.2024.09.042.

References

[1] K.M. Yamada, A.D. Doyle, J. Lu, Cell-3D matrix interactions: recent advances and opportunities, Trends Cell Biol. 32 (2022) 883–895, doi:10.1016/j.tcb.2022.03.002.
[2] S. Van Helvert, C. Storm, P. Friedl, Mechanoreciprocity in cell migration, Nat. Cell Biol. 20 (2017) 8–20, doi:10.1038/s41556-017-0012-0.
[3] C.E. Chan, D.J. Odde, Traction Dynamics of Filopodia on Compliant Substrates, Science 322 (2008) 1687–1691, doi:10.1126/science.1163595.
[4] H. Lee, L. Gu, D.J. Mooney, M.E. Levenston, O. Chaudhuri, Mechanical confinement regulates cartilage matrix formation by chondrocytes, Nat. Mater. 16 (2017) 1243–1251, doi:10.1038/nmat4993.
[5] H. pyo Lee, R. Stowers, O. Chaudhuri, Volume expansion and TRPV4 activation regulate stem cell fate in three-dimensional microenvironments, Nat. Commun. 10 (2019) 1–13, doi:10.1038/s41467-019-08465-x.
[6] J. Chang, A. Saraswathibhatla, Z. Song, S. Varma, C. Sanchez, N.H.K. Alyafei, D. Indana, R. Slyman, S. Srivastava, K. Liu, M.C. Bassik, M.P. Marinkovich, L. Hodgson, V. Shenoy, R.B. West, O. Chaudhuri, Cell volume expansion and local contractility drive collective invasion of the basement membrane in breast cancer, Nat. Mater. 2023 (2023) 1–12, doi:10.1038/s41563-023-01716-9.
[7] C.J. Walker, C. Crocini, D. Ramirez, A.R. Killaars, J.C. Grim, B.A. Aguado, K. Clark, M.A. Allen, R.D. Dowell, L.A. Leinwand, K.S. Anseth, Nuclear mechanosensing drives chromatin remodelling in persistently activated fibroblasts, Nat. Biomed. Eng. 512 (5) (2021) 1485–1499 2021, doi:10.1038/s41551-021-00709-w.
[8] J.A. Rowley, G. Madlambayan, D.J. Mooney, Alginate hydrogels as synthetic extracellular matrix materials, Biomaterials 20 (1999) 45–53, doi:10.1016/S0142-9612(98)00107-0.
[9] D. MacPherson, Y. Bram, J. Park, R.E. Schwartz, Peptide-based scaffolds for the culture and maintenance of primary human hepatocytes, Sci. Rep. 11 (2021) 1–9 2021 111, doi:10.1038/s41598-021-86016-5.
[10] J. Huang, R. Yang, J. Jiao, Z. Li, P. Wang, Y. Liu, S. Li, C. Chen, Z. Li, G. Qu, K. Chen, X. Wu, B. Chi, J. Ren, A click chemistry-mediated all-peptide cell printing hydrogel platform for diabetic wound healing, Nat. Commun. 141 (14) (2023) 1–20 2023, doi:10.1038/s41467-023-43364-2.

[11] H.R. Moreira, D.B. Rodrigues, S. Freitas-Ribeiro, L.P. da Silva, A. da S. Morais, M. Jarnalo, R. Horta, R.L. Reis, R.P. Pirraco, A.P. Marques, Integrin-specific hydrogels for growth factor-free vasculogenesis, Npj Regen. Med. 71 (7) (2022) 1–13 2022, doi:10.1038/s41536-022-00253-4.
[12] C. Ligorio, A. Mata, Synthetic extracellular matrices with function-encoding peptides, Nat. Rev. Bioeng. 17 (1) (2023) 518–536 2023, doi:10.1038/s44222-023-00055-3.
[13] P. Zarrintaj, S. Manouchehri, Z. Ahmadi, M.R. Saeb, A.M. Urbanska, D.L. Kaplan, M. Mozafari, Agarose-based biomaterials for tissue engineering, Carbohydr. Polym. 187 (2018) 66–84, doi:10.1016/J.CARBPOL.2018.01.060.
[14] J.Y. Xiong, J. Narayanan, X.Y. Liu, T.K. Chong, S.B. Chen, T.S. Chung, Topology evolution and gelation mechanism of agarose gel, J. Phys. Chem. B 109 (2005) 5638–5643, doi:10.1021/jp044473u.
[15] V. Normand, D.L. Lootens, E. Amici, K.P. Plucknett, P. Aymard, New insight into agarose gel mechanical properties, Biomacromolecules 1 (2000) 730–738, doi:10.1021/bm005583j.
[16] F. Piazza, P. Parisse, J. Passerino, E. Marsich, L. Bersanini, D. Porrelli, G. Baj, I. Donati, P. Sacco, Controlled quenching of agarose defines hydrogels with tunable structural, bulk mechanical, surface nanomechanical and cell response in 2d cultures, Adv. Healthc. Mater. 12 (2023) 2300973, doi:10.1002/ADHM.202300973.
[17] C.T. Buckley, S.D. Thorpe, F.J. O'Brien, A.J. Robinson, D.J. Kelly, The effect of concentration, thermal history and cell seeding density on the initial mechanical properties of agarose hydrogels, J. Mech. Behav. Biomed. Mater. 2 (2009) 512–521, doi:10.1016/J.JMBBM.2008.12.007.
[18] F. Piazza, P. Sacco, E. Marsich, G. Baj, F. Asaro, G. Grassi, M. Grassi, I. Donati, Cell activities on viscoelastic substrates show an elastic energy threshold and correlate with the linear elastic energy loss in the strain-softening region, Adv. Funct. Mater. 33 (2023) 2307224, doi:10.1002/adfm.202307224.
[19] M. Watase, K. Nishinari, Rheological properties of agarose gels with different molecular weights, Rheol. Acta 22 (1983) 580–587, doi:10.1007/BF01351404.
[20] M. Watase, K. Arakawa, Rheological properties of hydrogels of agar-agar. III. Stress relaxation of agarose gels, Bull. Chem. Soc. Jpn. 41 (1968) 1830–1834, doi:10.1246/BCSJ.41.1830.
[21] M.A. Krishnan, K. Yadav, V. Chelvam, Agarose micro-well platform for rapid generation of homogenous 3D tumor spheroids, Curr. Protoc. 1 (2021) e199, doi:10.1002/CPZ1.199.
[22] M. Li, T. Fu, S. Yang, L. Pan, J. Tang, M. Chen, P. Liang, Z. Gao, L. Guo, Agarose-based spheroid culture enhanced stemness and promoted odontogenic differentiation potential of human dental follicle cells *in vitro*, Vitr. Cell. Dev. Biol. - Anim. 57 (2021) 620–630, doi:10.1007/s11626-021-00591-5.
[23] X. Gong, C. Lin, J. Cheng, J. Su, H. Zhao, T. Liu, X. Wen, P. Zhao, Generation of multicellular tumor spheroids with microwell-based agarose scaffolds for drug testing, PLoS ONE 10 (2015) e0130348, doi:10.1371/journal.pone.0130348.
[24] M.C. Dodla, R.V. Bellamkonda, Differences between the effect of anisotropic and isotropic laminin and nerve growth factor presenting scaffolds on nerve regeneration across long peripheral nerve gaps, Biomaterials 29 (2008) 33–46, doi:10.1016/j.biomaterials.2007.08.045.
[25] Y. Luo, M.S. Shoichet, Light-activated immobilization of biomolecules to agarose hydrogels for controlled cellular response, Biomacromolecules 5 (2004) 2315–2323, doi:10.1021/BM0495811.
[26] Y. Luo, M.S. Shoichet, A photolabile hydrogel for guided three-dimensional cell growth and migration, Nat. Mater. 34 (3) (2004) 249–253 2004, doi:10.1038/nmat1092.
[27] Y. Yamada, C. Yoshida, K. Hamada, Y. Kikkawa, M. Nomizu, Development of three-dimensional cell culture scaffolds using laminin peptide-conjugated agarose microgels, Biomacromolecules 21 (2020) 3765–3771, doi:10.1021/acs.biomac.0c00871.
[28] Y. Yamada, K. Hozumi, A. Aso, A. Hotta, K. Toma, F. Katagiri, Y. Kikkawa, M. Nomizu, Laminin active peptide/agarose matrices as multifunctional biomaterials for tissue engineering, Biomaterials 33 (2012) 4118–4125, doi:10.1016/J.BIOMATERIALS.2012.02.044.
[29] N. Rahman, K.A. Purpura, R.G. Wylie, P.W. Zandstra, M.S. Shoichet, The use of vascular endothelial growth factor functionalized agarose to guide pluripotent stem cell aggregates toward blood progenitor cells, Biomaterials 31 (2010) 8262–8270, doi:10.1016/J.BIOMATERIALS.2010.07.040.
[30] P. Sacco, F. Piazza, C. Pizzolitto, G. Baj, F. Brun, E. Marsich, I. Donati, Regulation of substrate dissipation via tunable linear elasticity controls cell activity, Adv. Funct. Mater. 32 (2022) 2200309, doi:10.1002/ADFM.202200309.
[31] E.G. Hayman, E. Ruoslahti, Distribution of fetal bovine serum fibronectin and endogenous rat cell fibronectin in extracellular matrix, J. Cell Biol. 83 (1979) 255–259, doi:10.1083/JCB.83.1.255.
[32] E.G. Hayman, M.D. Pierschbacher, S. Suzuki, E. Ruoslahti, Vitronectin-a major cell attachment-promoting protein in fetal bovine serum, Exp. Cell Res. 160 (1985) 245–258, doi:10.1016/0014-4827(85)90173-9.
[33] X. Zheng, H. Baker, W.S. Hancock, F. Fawaz, M. McCaman, E. Pungor, Proteomic analysis for the assessment of different lots of fetal bovine serum as a raw material for cell culture. Part IV. Application of proteomics to the manufacture of biological drugs, Biotechnol. Prog. 22 (2006) 1294–1300, doi:10.1021/BP060121O.
[34] A.M. Merlot, D.S. Kalinowski, D.R. Richardson, Unraveling the mysteries of serum albumin-more than just a serum protein, Front. Physiol. 5 (2014) 299, doi:10.3389/fphys.2014.00299.
[35] S.I. Aota, M. Nomizu, K.M. Yamada, The short amino acid sequence Pro-His-Ser-Arg-Asn in human fibronectin enhances cell-adhesive function, J. Biol. Chem. 269 (1994) 24756–24761, doi:10.1016/S0021-9258(17)31456-4.
[36] J.E. Koblinski, M. Wu, B. Demeler, K. Jacob, H.K. Kleinman, Matrix cell adhesion activation by non-adhesion proteins, J. Cell Sci. 118 (2005) 2965–2974, doi:10.1242/JCS.02411.
[37] M.P.M. Soutar, L. Kempthorne, E. Annuario, C. Luft, S. Wray, R. Ketteler, M.H.R. Ludtmann, H. Plun-Favreau, FBS/BSA media concentration determines CCCP's ability to depolarize mitochondria and activate PINK1-PRKN mitophagy, Autophagy 15 (2019) 2002, doi:10.1080/15548627.2019.1603549.
[38] T. Singh, R. Meena, A. Kumar, Effect of sodium sulfate on the gelling behavior of agarose and water structure inside the gel networks, J. Phys. Chem. B 113 (2009) 2519–2525, doi:10.1021/jp809294p.
[39] J.T. Connelly, T.A. Petrie, A.J. García, M.E. Levenston, Fibronectin- and collagen-mimetic ligands regulate BMSC chondrogenesis in 3D hydrogels, Eur. Cell. Mater. 22 (2011) 168, doi:10.22203/ecm.v022a13.
[40] P. Sacco, F. Furlani, S. Paoletti, I. Donati, PH-assisted gelation of lactose-modified chitosan, Biomacromolecules 20 (2019), doi:10.1021/acs.biomac.9b00636.
[41] G. Turco, I. Donati, M. Grassi, G. Marchioli, R. Lapasin, S. Paoletti, Mechanical spectroscopy and relaxometry on alginate hydrogels: a comparative analysis for structural characterization and network mesh size determination, Biomacromolecules 12 (2011) 1272–1282, doi:10.1021/bm101556m.
[42] O. Chaudhuri, L. Gu, D. Klumpers, M. Darnell, S.A. Bencherif, J.C. Weaver, N. Huebsch, H. Lee, E. Lippens, G.N. Duda, D.J. Mooney, Hydrogels with tunable stress relaxation regulate stem cell fate and activity, Nat. Mater. 15 (2016) 326–334, doi:10.1038/nmat4489.
[43] T.J. Stefonek, K.S. Masters, Immobilized gradients of epidermal growth factor promote accelerated and directed keratinocyte migration, Wound Repair Regen. 15 (2007) 847–855, doi:10.1111/J.1524-475X.2007.00288.X.
[44] J. Seong, A. Tajik, J. Sun, J.L. Guan, M.J. Humphries, S.E. Craig, A. Shekaran, A.J. García, S. Lu, M.Z. Lin, N. Wang, Y. Wang, Distinct biophysical mechanisms of focal adhesion kinase mechanoactivation by different extracellular matrix proteins, Proc. Natl. Acad. Sci. U.S.A. 110 (2013) 19372–19377, doi:10.1073/PNAS.1307405110.
[45] M.J. Halvorson, J.E. Coligan, K. Sturmhöfel, The vitronectin receptor (alpha V beta 3) as an example for the role of integrins in T lymphocyte stimulation, Immunol. Res. 15 (1996) 16–29, doi:10.1007/BF02918281.
[46] I. Tsagaraki, E.C. Tsilibary, A.K. Tzinia, TIMP-1 interaction with $\alpha v\beta 3$ integrin confers resistance to human osteosarcoma cell line MG-63 against TNF-α-induced apoptosis, Cell Tissue Res. 342 (2010) 87–96, doi:10.1007/S00441-010-1025-1.
[47] K.T. Preissner, D. Seiffert, Role of vitronectin and its receptors in haemostasis and vascular remodeling, Thromb. Res. 89 (1998) 1–21, doi:10.1016/S0049-3848(97)00298-3.
[48] D. Seiffert, J.W. Smith, The cell adhesion domain in plasma vitronectin is cryptic, J. Biol. Chem. 272 (1997) 13705–13710, doi:10.1074/JBC.272.21.13705.
[49] A. Stockmann, S. Hess, P. Declerck, R. Timpl, K.T. Preissner, Multimeric vitronectin. Identification and characterization of conformation-dependent self-association of the adhesive protein, J. Biol. Chem. 268 (1993) 22874–22882, doi:10.1016/S0021-9258(18)41608-0.
[50] Y. Yang, X. Liu, W. Yu, H. Zhou, X. Li, X. Ma, Homogeneous synthesis of GRGDY grafted chitosan on hydroxyl groups by photochemical reaction for improved cell adhesion, Carbohydr. Polym. 80 (2010) 733–739, doi:10.1016/J.CARBPOL.2009.12.019.
[51] S.D. Redick, D.L. Settles, G. Briscoe, H.P. Erickson, Defining fibronectin's cell adhesion synergy site by site-directed mutagenesis, J. Cell Biol. 149 (2000) 521, doi:10.1083/JCB.149.2.521.
[52] J.C. Friedland, M.H. Lee, D. Boettiger, Mechanically activated integrin switch controls $\alpha 5\beta$ 1 function, Science 323 (2009) 642–644, doi:10.1126/science.1168441.